Supporting Information

A New Route to Porous Metal-Organic Framework Crystal-Glass Composites

Shichun Li [a, b], Shuwen Yu [a, c], Sean M. Collins [b], Duncan N. Johnstone [b], Christopher W. Ashling [b], Adam F. Sapnik [b], Philip A. Chater [d], Dean S. Keeble [d], Lauren N. McHugh [b], Paul A. Midgley [b], David. A. Keen [e], and Thomas D. Bennett [b, *]

a. Institute of Chemical Materials, China Academy of Engineering Physics, Mianyang 621900, P. R. China.

b. Department of Materials Science and Metallurgy, University of Cambridge, 27 Charles Babbage Road, Cambridge CB3 0FS, United Kingdom.

c. Xiamen Institute of Rare Earth Materials, Haixi Institute, Chinese Academy of Sciences, Xiamen 361021, P. R. China.

d. Diamond House, Harwell Science & Innovation Campus, Diamond Light Source, Ltd., Didcot, Oxfordshire OX11 0DE, United Kingdom.

e. ISIS Facility, Rutherford Appleton Laboratory, Harwell Campus, Didcot, Oxon OX11 0QX, United Kingdom.

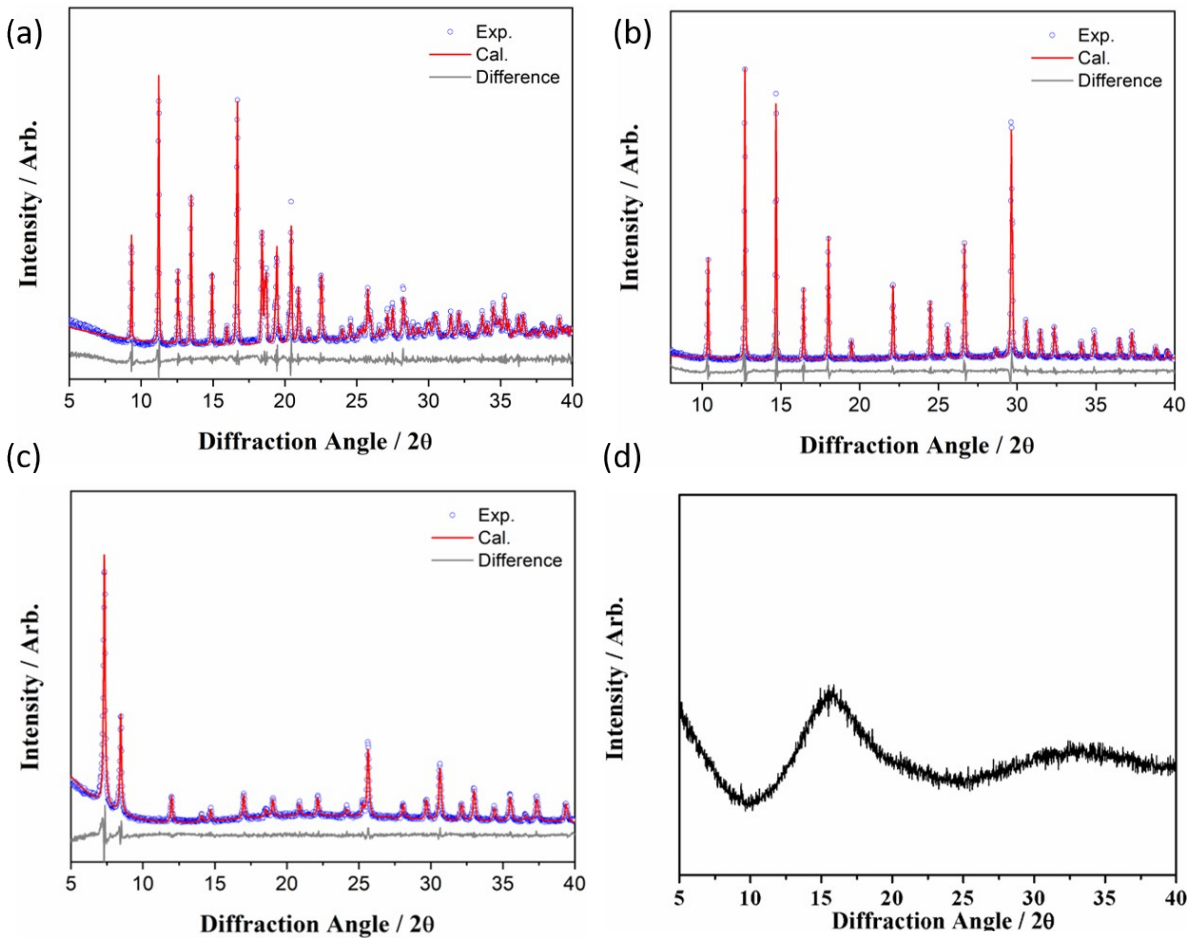

Figure S1. Pawley refinements of (a) ZIF-62, (b) ZIF-67 and (c) UiO-66 XRD patterns, using published structural parameters. [1, 2] (d) XRD pattern of a_gZIF-62.

Table S1. Lattice parameters of ZIF-62, ZIF-67 and UiO-66 obtained by Pawley refinement, and those reported in the literature [1, 2]. The starting values for the refinements were taken from the cell parameters reported in the literature.

	R_{wp}	Space Group	a/ Å	b/ Å	c/ Å	α	β	γ
Reported ZIF-62 [1]	-	*Pbca*	15.6620(14)	15.6621(13)	18.207 (2)	90°	90°	90°
ZIF-62	9.811		15.5892(13)	15.765(2)	18.2429(14)	90°	90°	90°
Reported ZIF-67 [1]	-	*I-43m*	16.9589(3)	16.9589(3)	16.9589(3)	90°	90°	90°
ZIF-67	9.992		17.0298(4)	17.0298(4)	17.0298(4)	90°	90°	90°
Reported UiO-66 [2]	-	*Fm-3m*	20.7551(5)	20.7551(5)	20.7551(5)	90°	90°	90°
UiO-66	8.534		20.819(3)	20.819(3)	20.819(3)	90°	90°	90°

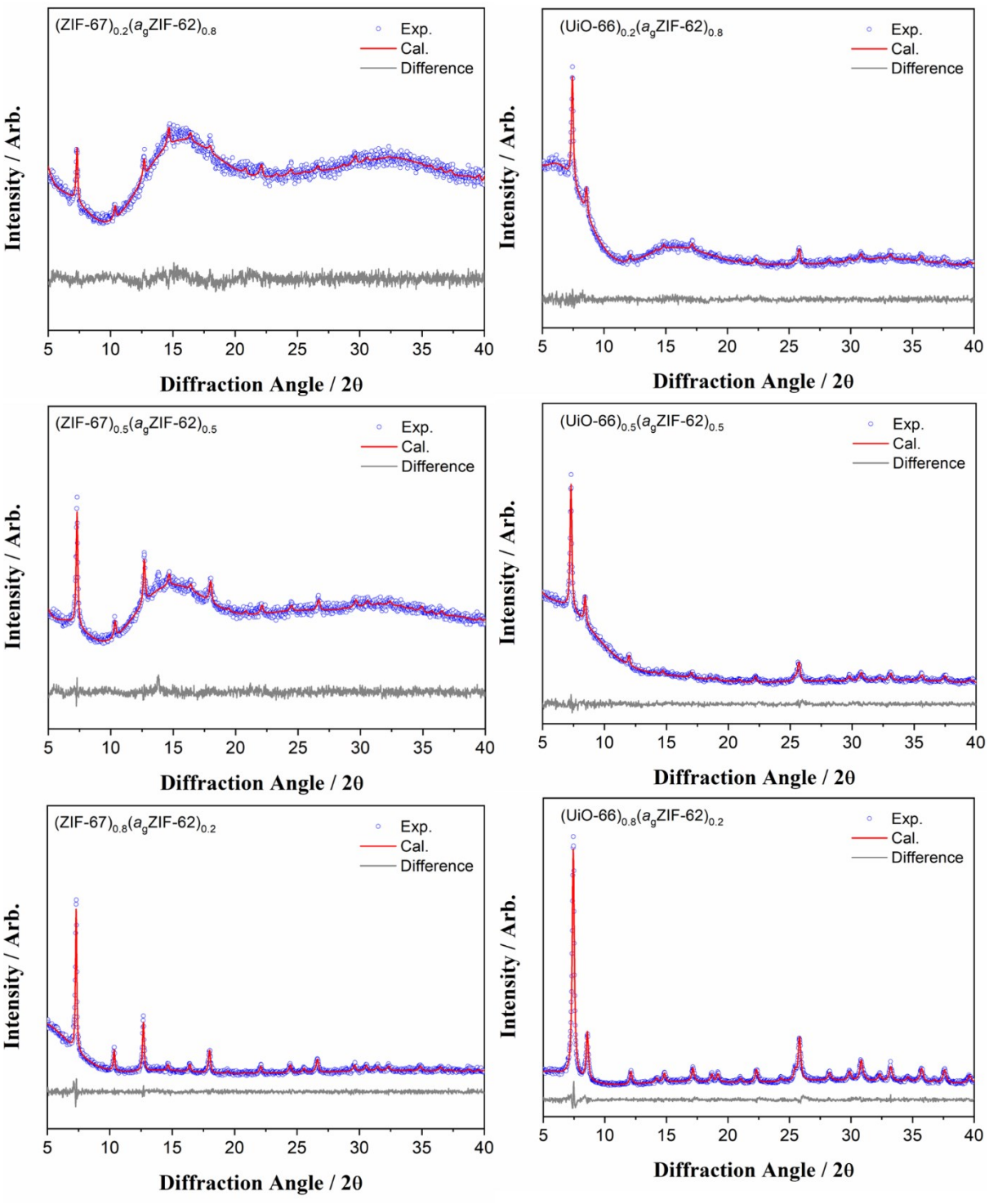

Figure S2. Pawley refinements of CGCs with ZIF-67 and UiO-66. The signal/noise ratio is relatively poor for both lower weight loadings of the ZIF-67 composite, and the lowest weight loading of UiO-66.

Table S2. Lattice parameters of ZIF-67 and UiO-66 obtained by Pawley refinement, and those reported in the literature [1, 2]. The starting values for the refinements were taken from the cell parameters reported in the literature.

	R_{wp}	Space Group	a/ Å	b/ Å	c/ Å	α	β	γ
Reported ZIF-67 [1]	-	*I-43m*	16.9589(3)	16.9589(3)	16.9589(3)	90°	90°	90°
$(ZIF\text{-}67)_{0.2}(a_gZIF\text{-}62)_{0.8}$	4.270		16.984(9)	16.984(9)	16.984(9)	90°	90°	90°
$(ZIF\text{-}67)_{0.5}(a_gZIF\text{-}62)_{0.5}$	4.118		17.113 (2)	17.113 (2)	17.113 (2)	90°	90°	90°
$(ZIF\text{-}67)_{0.8}(a_gZIF\text{-}62)_{0.2}$	8.905		17.090(1)	17.090(1)	17.090(1)	90°	90°	90°
Reported UiO-66 [2]	-	*Fm-3m*	20.7551(5)	20.7551(5)	20.7551(5)	90°	90°	90°
$(UiO\text{-}66)_{0.2}(a_gZIF\text{-}62)_{0.8}$	4.283		20.74(2)	20.74(2)	20.74(2)	90°	90°	90°
$(UiO\text{-}66)_{0.5}(a_gZIF\text{-}62)_{0.5}$	4.549		20.680(4)	20.680(4)	20.680(4)	90°	90°	90°
$(UiO\text{-}66)_{0.8}(a_gZIF\text{-}62)_{0.2}$	5.841		20.722(3)	20.722(3)	20.722(3)	90°	90°	90°

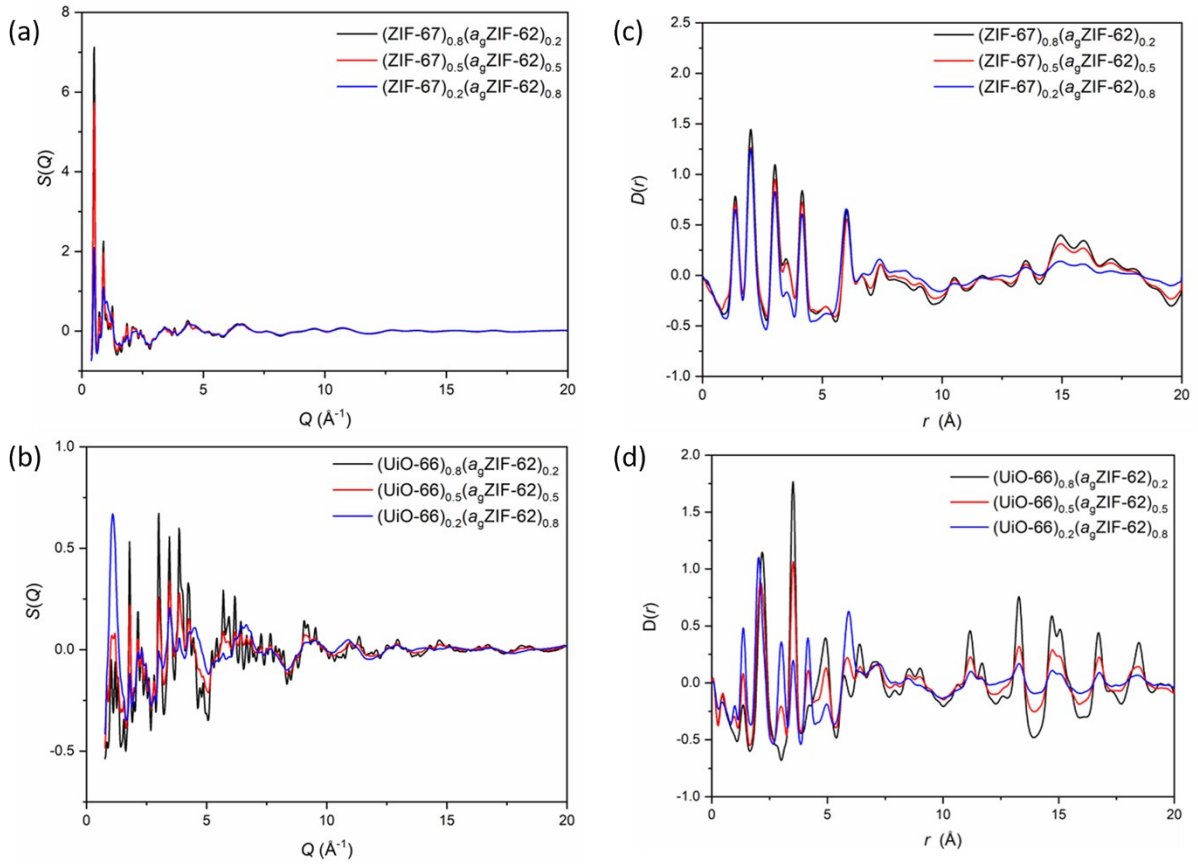

Figure S3. (a, b) Structure factors, *S*(*Q*), of CGCs with ZIF-67 and UiO-66. (c, d) Corresponding pair distribution functions, *D*(*r*).

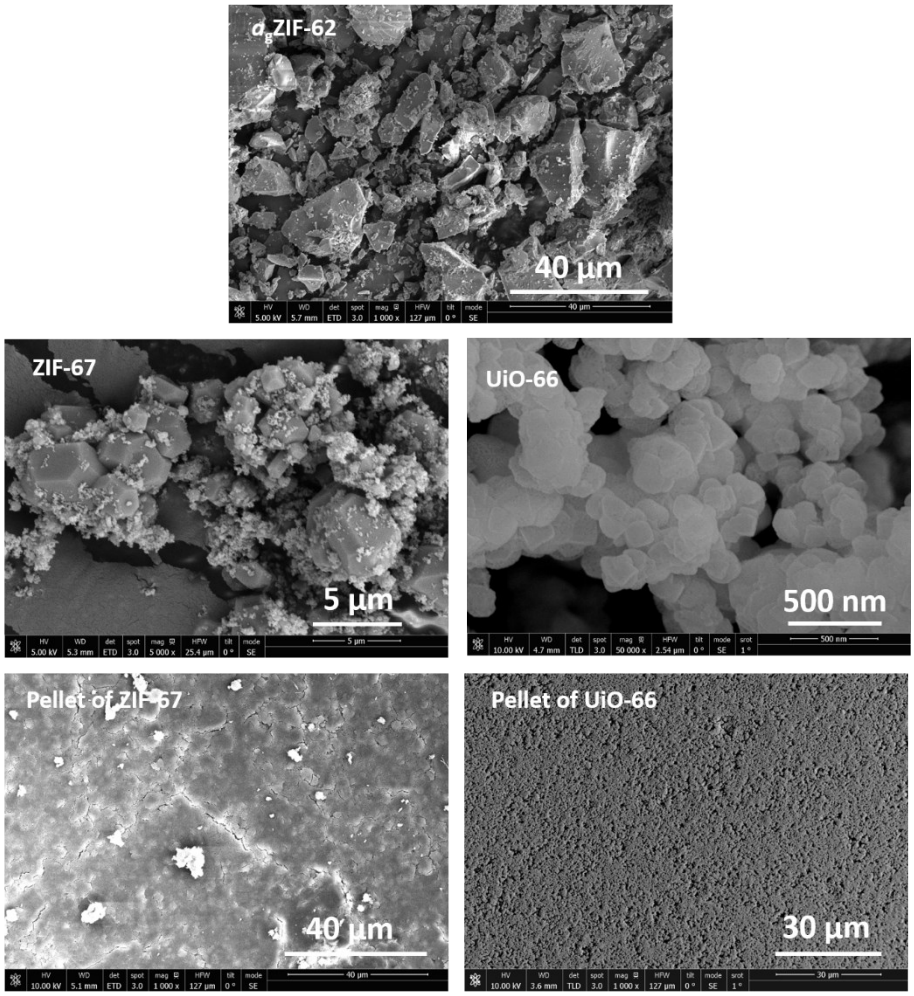

Figure S4. SEM images of a_gZIF-62, ZIF-67, and UiO-66.

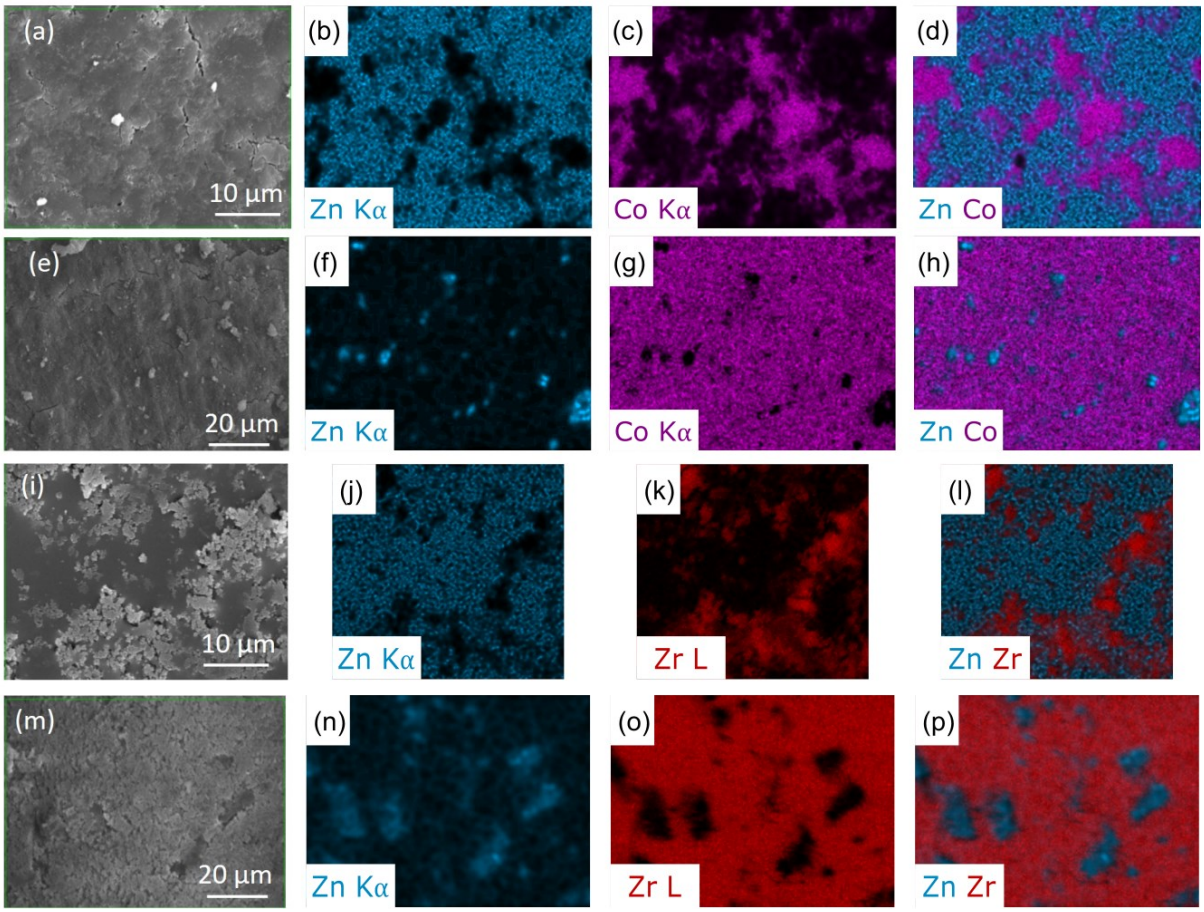

Figure S5. SEM images and EDX mappings of metal elements on the surface of CGCs (a -d) (ZIF-67)$_{0.2}$(a_gZIF-62)$_{0.8}$, (e-h) (ZIF-67)$_{0.5}$(a_gZIF-62)$_{0.5}$, (i-l) (ZIF-67)$_{0.8}$(a_gZIF-62)$_{0.2}$, (m-p) (UiO-66)$_{0.2}$(a_gZIF-62)$_{0.8}$.

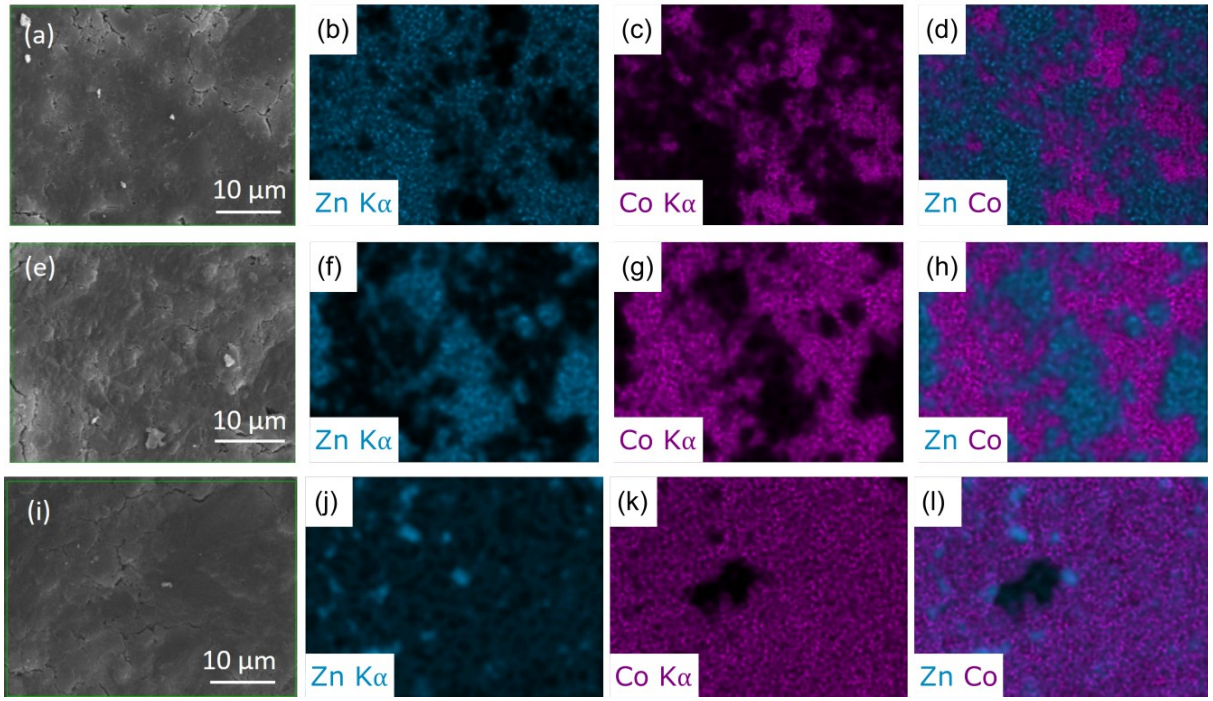

Figure S6. SEM images and EDX mappings of metal elements on the surface of (a -d) (ZIF-67)(a_gZIF-62)(20/80), (e-h) (ZIF-67)(a_gZIF-62)(50/50), and (i-l) (ZIF-67)(a_gZIF-62)(80/20).

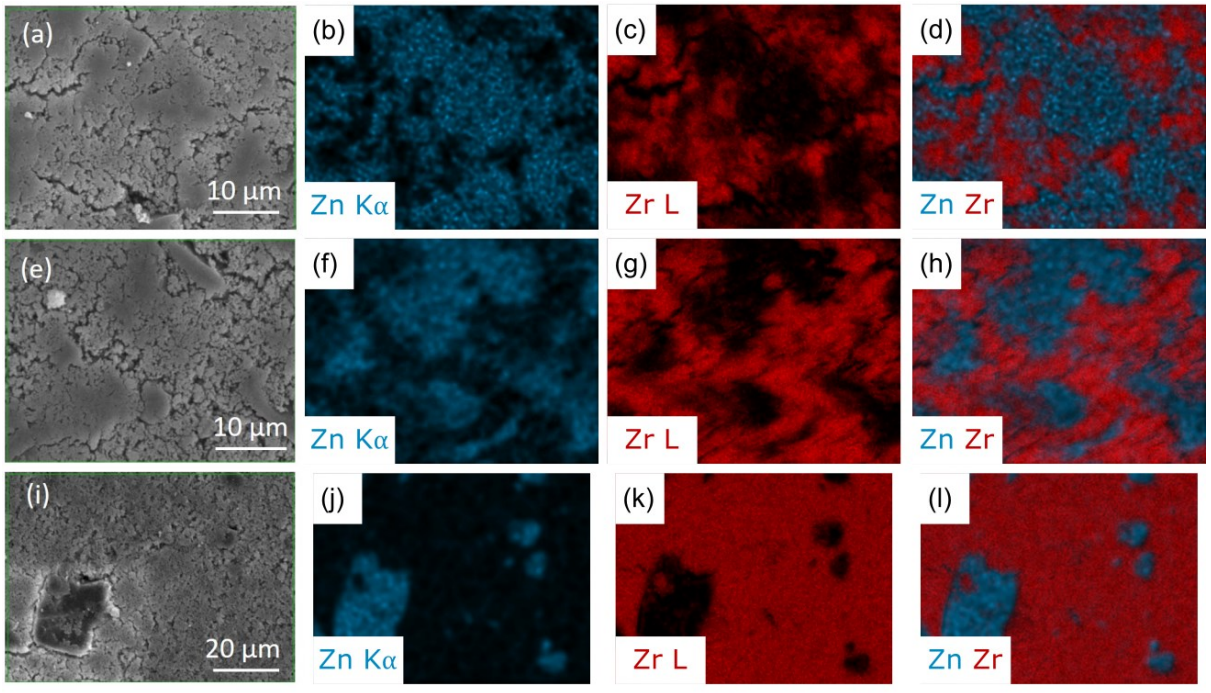

Figure S7. SEM images and EDX mappings of metal elements on the surface of (a -d) (UiO-66)(a_gZIF-62)(20/80), (e-h) (UiO-66)(a_gZIF-62)(50/50), and (i-l) (UiO-66)(a_gZIF-62)(80/20).

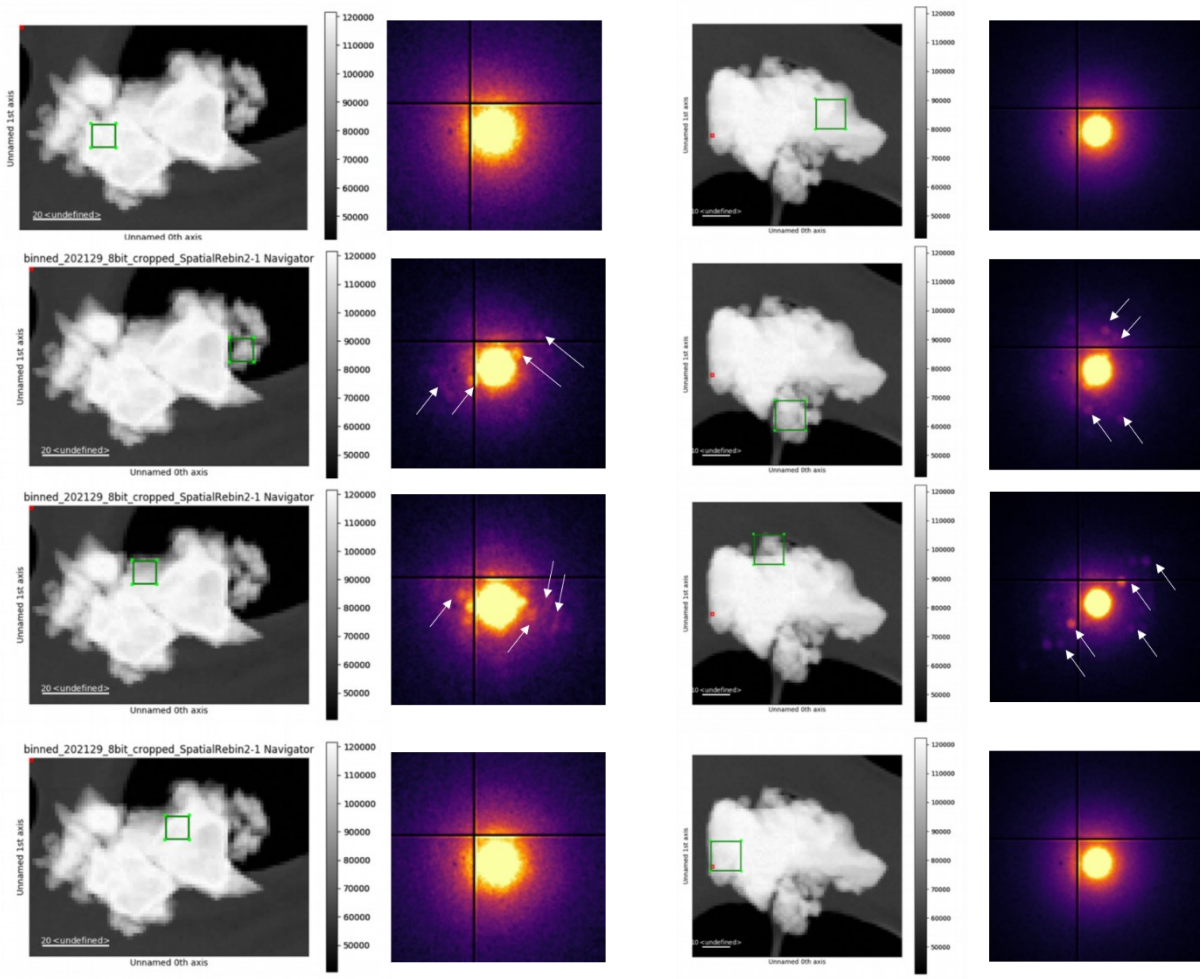

Figure S8. Validation of Bragg scattering in the selected region of CGC $(ZIF\text{-}67)_{0.5}(ZIF\text{-}62)_{0.5}$ tested with electron diffraction. White arrows mark some of the Bragg peaks.

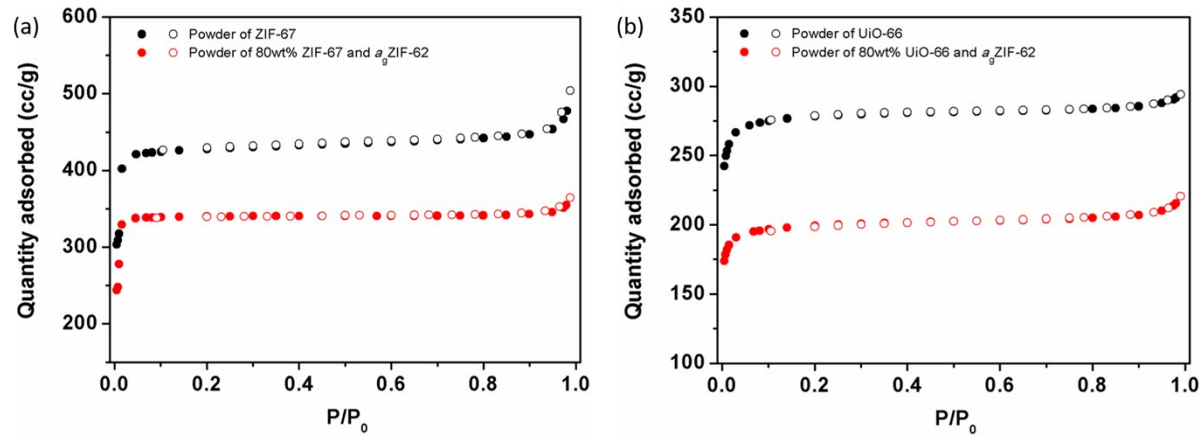

Figure S9. N_2 gas isotherms at 77K of (a) powders with ZIF-67, and (b) powders with UiO-66. Solid circles represent adsorption, and hollow circles represent desorption.

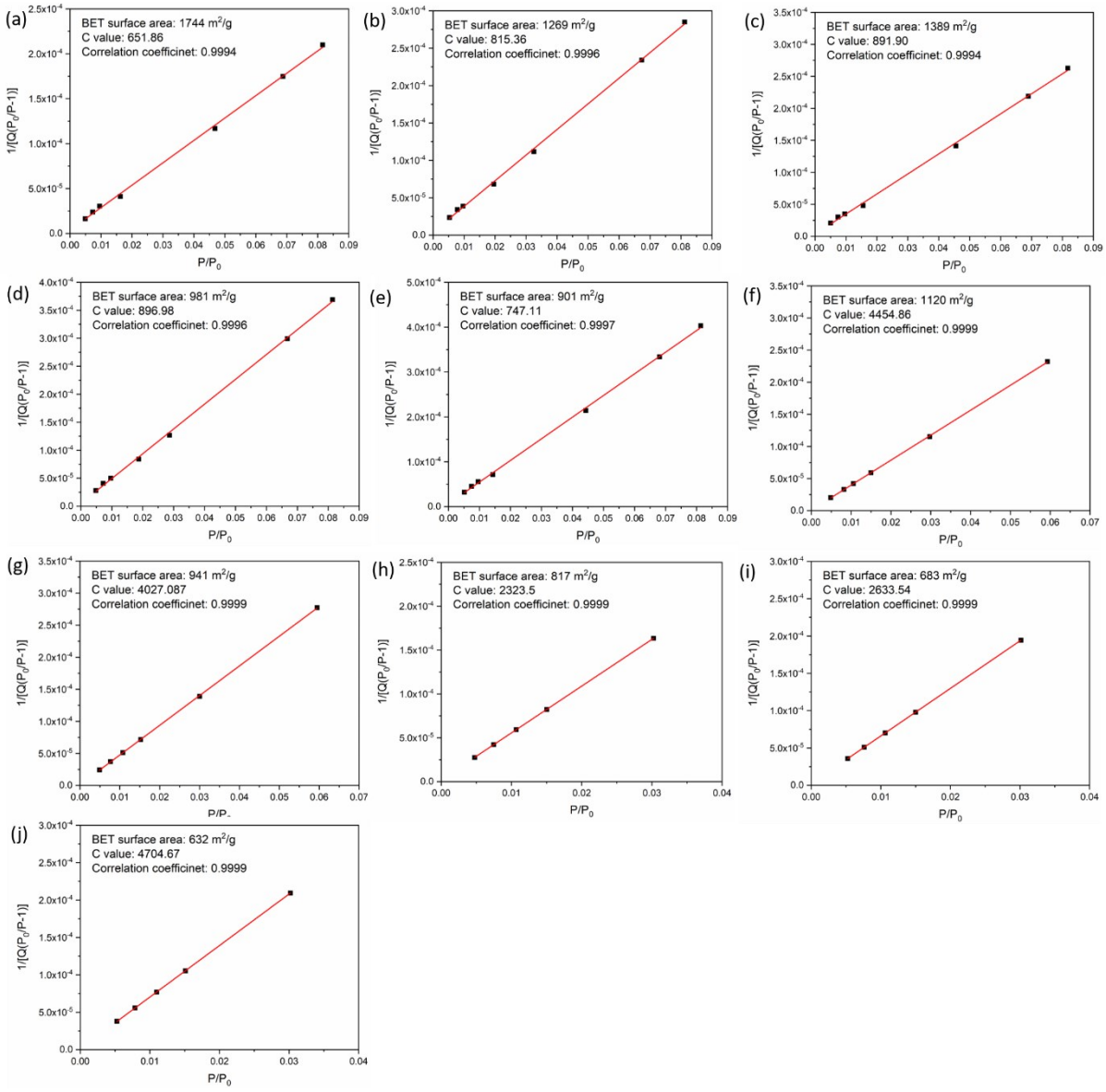

Figure S10. Calculation of BET surface area of (a) ZIF-67 powder, (b) ZIF-67 pellet, (c) powder of 80 wt% ZIF-67 and a_gZIF-62, (d) (ZIF-67)(a_gZIF-62)(80/20), (e) (ZIF-67)$_{0.8}$(a_gZIF-62)$_{0.2}$, (f) UiO-66 powder, (g) UiO-66 pellet, (h) powder of 80 wt% UiO-66 and a_gZIF-62, (i) (UiO-66)(a_gZIF-62)(80/20), (j) (UiO-66)$_{0.8}$(a_gZIF-62)$_{0.2}$.

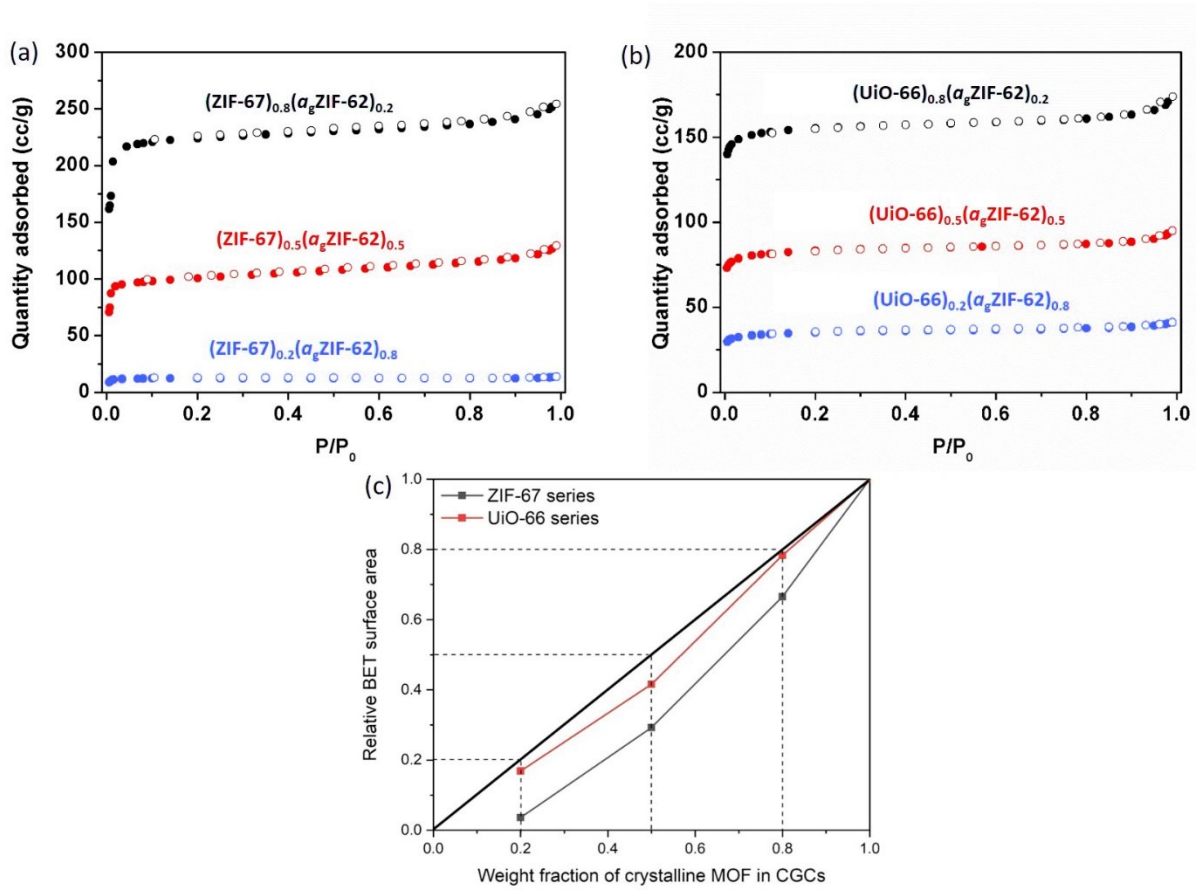

Figure S11. N_2 gas isotherms at 77K of (a) CGCs with ZIF-67, and (b) CGCs with UiO-66. Solid circles represent adsorption, and hollow circles represent desorption. (c) The relative BET surface area of CGCs with different weight fraction of crystalline MOF in CGCs. The relative BET surface area is the ratio of BET surface area of the CGC to that of the pellet of pure crystalline MOF after heating at 400 °C for 5 hours under Ar.

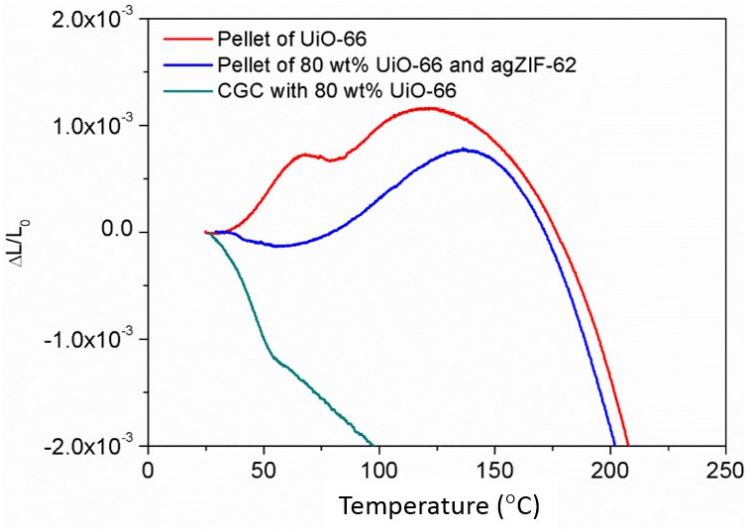

Figure S12. Thermal expansion of UiO-66 series tested by TMA. The non-physical result for the UiO-66 sample is consistent with the non-uniform nature of the sample and the presence of macroscale defects within the bulk solid (Figure 3e, S4, and S7i). The deformation of the $(UiO\text{-}66)_{0.8}(ZIF\text{-}62)_{0.2}$ sample, which is clear from the start of measurement, is ascribed to the dehydroxlyation of UiO-66 during the formation process.

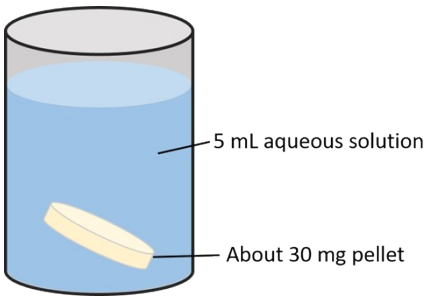

Figure S13. Schematic diagram of chemical stability experiments. The vail containing aqueous solution and sample was kept at room temperature for 7 days.

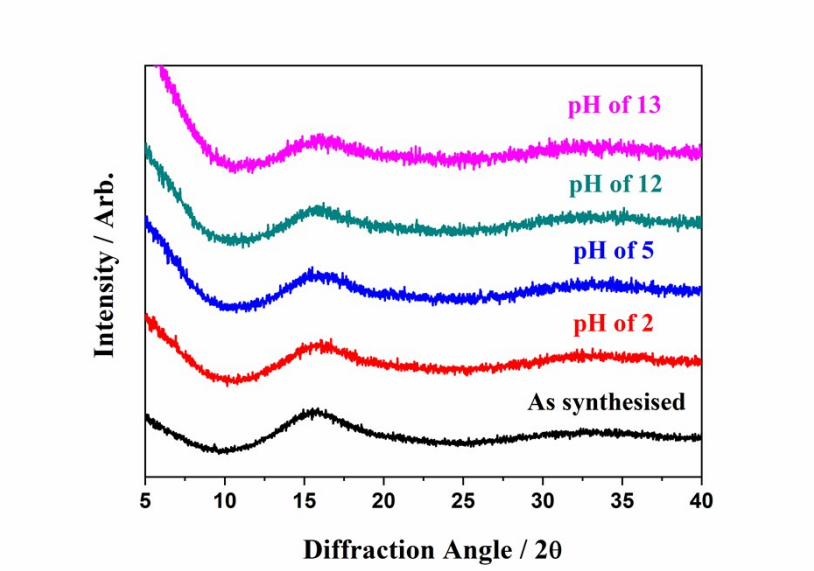

Figure S14. XRD pattern of a_gZIF-62 before and after soaking in aqueous acid and base.

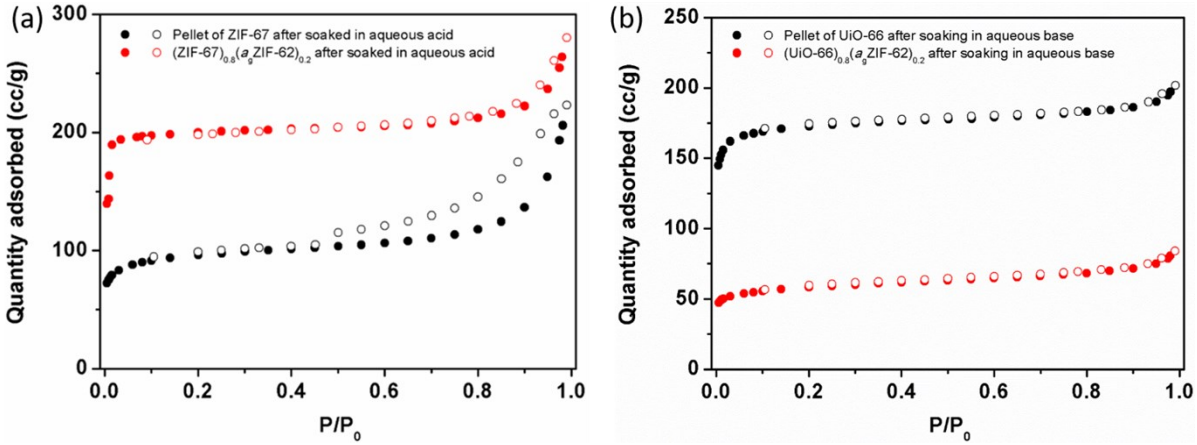

Figure S15. N_2 gas isotherms at 77K of pellets and CGCs with (a) ZIF-67 and (b) UiO-66 before and after soaking in aqueous acid at pH 5 or base at pH 12. Solid circles represent adsorption, and hollow circles represent desorption.

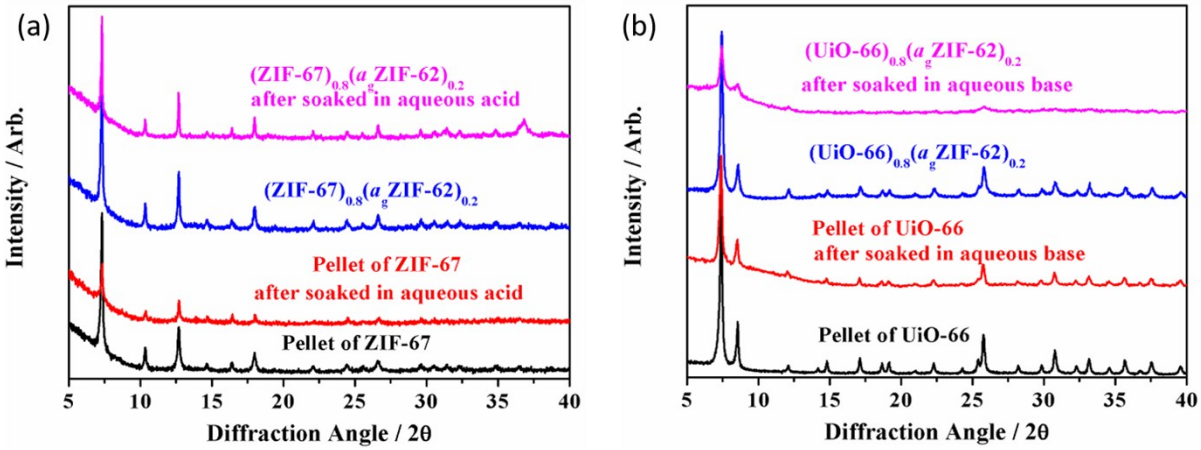

Figure S16. XRD pattern of pellets and CGCs with (a) ZIF-67 and (b) UiO-66 before and after soaking in aqueous acid at pH of 5 or base at pH of 12.

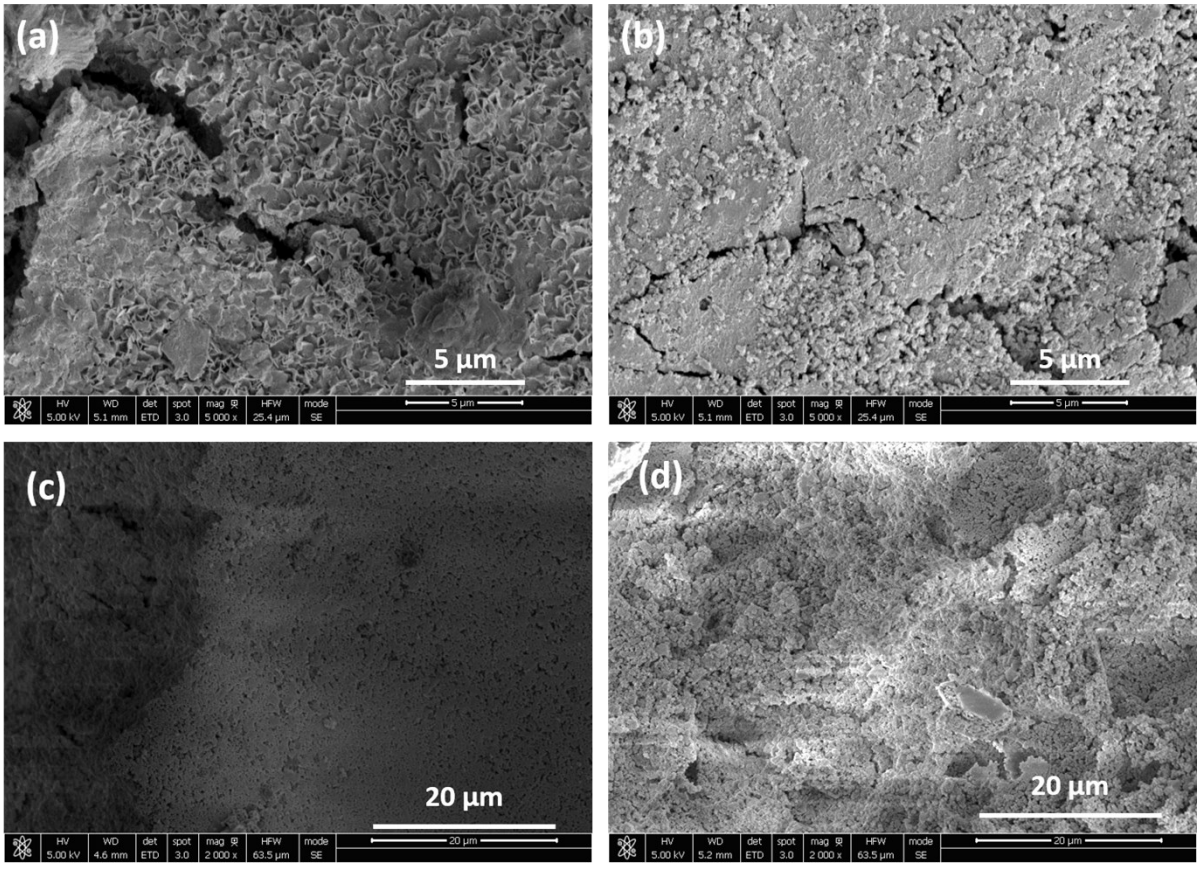

Figure S17. SEM images of (a) pellet of ZIF-67, (b) $(ZIF\text{-}67)_{0.8}(a_gZIF\text{-}62)_{0.2}$, (c) pellet of UiO-66, and $(UiO\text{-}66)_{0.8}(a_gZIF\text{-}62)_{0.2}$ after soaking in aqueous acid at pH 5 or base at pH 12.

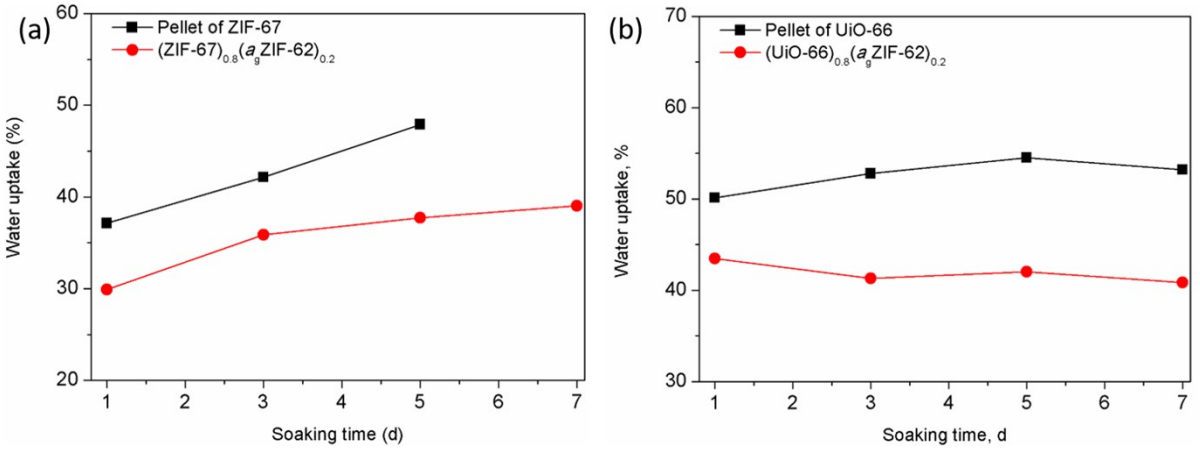

Figure S18. Water uptake at room temperature of pellets and CGCs with (a) ZIF-67 and (b) UiO-66. The pellet of ZIF-67 was broken after soaking for 7 days. The water uptake is calculated as follows:

$$Water\ uptake = \frac{W_b - W_a}{W_a \times \varphi} \times 100\% \quad (1)$$

where W_a is the weight of dry sample, W_b is the weight of wet sample, and φ is the weight fraction of MOF crystals in the dry sample.

References

1. R. Banerjee, A. Phan, B. Wang, C. Knobler, H. Furukawa, M. O'Keeffe and O. M. Yaghi, *Science*, 2008, **319**, 939-943.
2. J. H. Cavka, S. Jakobsen, U. Olsbye, N. Guillou, C. Lamberti, S. Bordiga and K. P. Lillerud, *J. Am. Chem. Soc.*, 2008, **130**, 13850-13851.